Supplementary materials

Minh-Quyet Ha,[1] Duong-Nguyen Nguyen,[1] Viet-Cuong Nguyen,[2] Takahiro Nagata,[3] Toyohiro Chikyow,[4] Hiori Kino,[4] Takashi Miyake,[5] Thierry Denœux,[6] Van-Nam Huynh,[1] and Hieu-Chi Dam[1, a)]

[1)] *Japan Advanced Institute of Science and Technology, 1-1 Asahidai, Nomi, Ishikawa 923-1292, Japan*

[2)] *HPC SYSTEMS Inc., Minato, Tokyo 108-0022, Japan*

[3)] *RCFM, National Institute for Materials Science, 1-2-1 Sengen, Tsukuba, Ibaraki 305-0044, Japan*

[4)] *MaDIS, National Institute for Materials Science, 1-2-1 Sengen, Tsukuba, Ibaraki 305-0047, Japan*

[5)] *CD-FMat, AIST, 1-1-1 Umezono, Tsukuba, Ibaraki 305-8568, Japan*

[6)] *Université de technologie de Compiègne, CNRS, UMR 7253 Heudiasyc, Compiègne, France*

(Dated: 23 January 2021)

I. ALLOYS DATA SETS

In the evaluation experiments, we use eight data sets consisting of binary, ternary, quaternary, and quinary alloys comprising multiple equiatomically combined elements. The data sets consist of data from experiments and calculations. The alloys contained in the data sets comprise $\mathcal{E} = \{$ Fe, Co, Ir, Cu, Ni, Pt, Pd, Rh, Au, Ag, Ru, Os, Si, As, Al, Tc, Re, Mn, Ta, Ti, W, Mo, Cr, V, Hf, Nb, and Zr$\}$. Figure 1 shows the proportion of 27 elements in the data sets. Any alloy contained in the following data sets is predicted as an HEA if its order-disorder transition temperature is below its melting temperature.

- $\mathcal{D}_{\text{ASMI16}}$: The order-disorder transition temperatures (T_c^{exp}) and melting temperatures (T_m^{exp}) of the alloys are both experimentally evaluated[1]. All of the alloys contained in $\mathcal{D}_{\text{ASMI16}}$ show an order-disorder transition temperature below their melting temperature ($T_c^{\text{exp}} < T_m^{\text{exp}}$).

- $\mathcal{D}_{\text{CALPHAD}}$: The order-disorder transition temperatures ($T_c^\star$) and melting temperatures ($T_m^\star$) of the alloys are both predicted using calculated-phase-diagram (CALPHAD) calculations[2–4] based on the temperatures for some binary alloys (three possible for each ternary alloy) found in the Thermo-Calc software SSOL5 database[5]. Similar to the $\mathcal{D}_{\text{ASMI16}}$ data set, the $\mathcal{D}_{\text{CALPHAD}}$ data set only contains the alloys satisfying $T_c^\star < T_m^\star$.

- $\mathcal{D}_{\text{AFLOW}}$, $\mathcal{D}_{\text{AFLOW}}^{\text{quaternary}}$, and $\mathcal{D}_{\text{AFLOW}}^{\text{quinary}}$: The order-disorder transition temperatures (T_c^{AFLOW}) of the alloys contained in these data sets are estimated using the automatic flow (AFLOW) convex-hull database[6]. The melting temperatures T_m^{exp} and $T_m^\star$ are applied to the binary and ternary alloys, respectively. The alloy is considered as an HEA if $T_c^{\text{AFLOW}} < T_m^{\text{exp}}$ for binary alloys and $T_c^{\text{AFLOW}} < T_m^\star$ for ternary, quaternary, and quinary alloys).

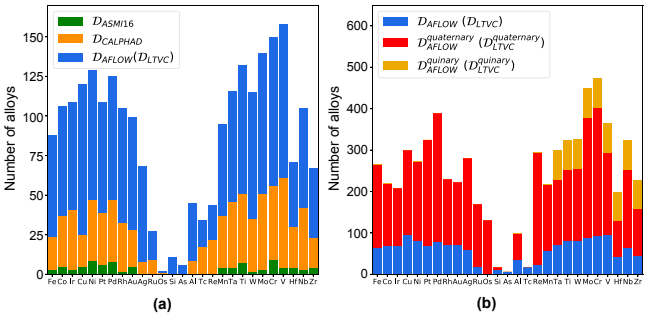

FIG. 1. Proportions of 27 elements in $\mathcal{D}_{\text{ASMI16}}$, $\mathcal{D}_{\text{CALPHAD}}$, $\mathcal{D}_{\text{AFLOW}}$, $\mathcal{D}_{\text{AFLOW}}^{\text{quaternary}}$, $\mathcal{D}_{\text{AFLOW}}^{\text{quinary}}$, $\mathcal{D}_{\text{LTVC}}$, $\mathcal{D}_{\text{LTVC}}^{\text{quaternary}}$, and $\mathcal{D}_{\text{LTVC}}^{\text{quinary}}$ data sets.

- $\mathcal{D}_{\text{LTVC}}$, $\mathcal{D}_{\text{LTVC}}^{\text{quaternary}}$, and $\mathcal{D}_{\text{LTVC}}^{\text{quinary}}$: These data sets contain the same alloys as those contained in data sets $\mathcal{D}_{\text{AFLOW}}$, $\mathcal{D}_{\text{AFLOW}}^{\text{quaternary}}$, and $\mathcal{D}_{\text{AFLOW}}^{\text{quinary}}$, respectively. However, the properties of the alloys contained in these data sets are predicted using the method of Lederer, Toher, Vecchio, and Curtarolo (LTVC)[7]. *Ab-initio* calculations are used to estimate the order-disorder transition temperatures (T_c^{LTVC}) of the alloys contained in these data sets. In addition, the T_m values are the same as those of the alloys contained in the AFLOW data sets. Any alloy in these data sets is predicted as an HEA if $T_c^{\text{LTVC}} < T_m^{\text{exp}}$ for binary alloys and $T_c^{\text{LTVC}} < T_m^\star$ for ternary, quaternary, and quinary alloys

Note that $\mathcal{D}_{\text{ASMI16}}$ and $\mathcal{D}_{\text{CALPHAD}}$ only contain confirmed and predicted HEAs, respectively. Therefore, although we assume that the properties of all the other binary or ternary alloys (not included in the data set) have not yet been confirmed, we do not assume that those alloys are not HEAs.

II. MATERIALS DESCRIPTORS

Descriptors, which are the representation of alloys, play a crucial role in building a recommender system to

[a)] Electronic mail: dam@jaist.ac.jp

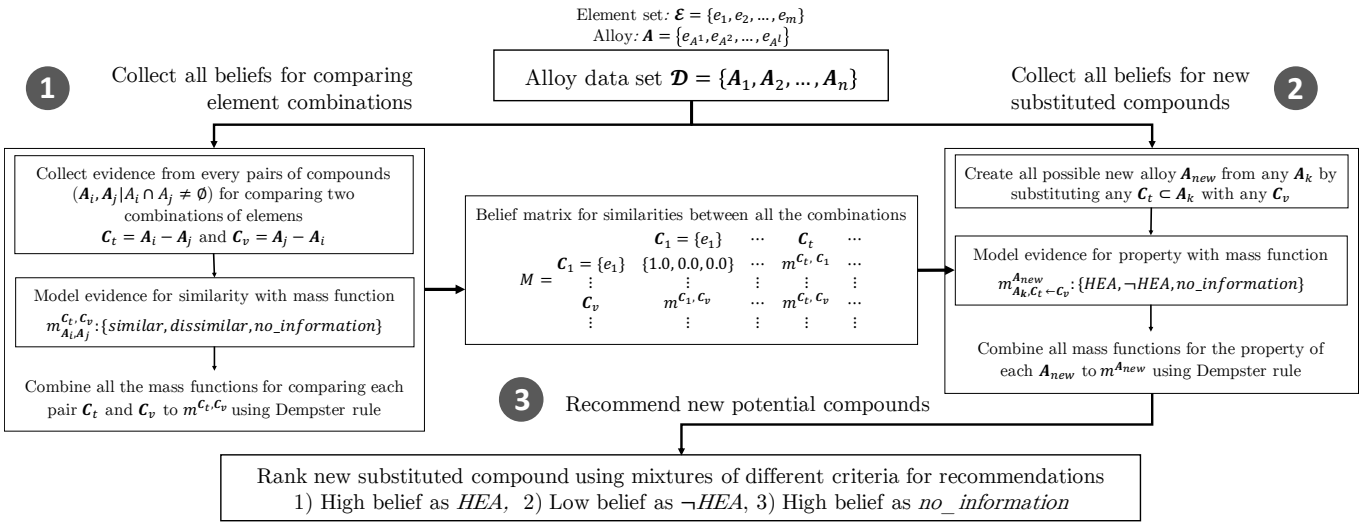

FIG. 2. Workflow chart illustrating three ERS stages required for recommending undiscovered HEAs. The data set $\mathcal{D}$ includes observed materials generated from a finite set $\mathcal{E}$ of elements.

explore potential new HEAs. In this research, the raw data of alloys is represented in the form of elements combination. Several descriptors have been studied in materials informatics to represent the compounds[8]. To employ the data-driven approaches for this work, we applied compositional descriptor[9], rating matrix representation[10] and binary elemental descriptor[8].

Compositional descriptor represents an alloy by a set of 135 features composed of means, standard deviations, and covariance of established atomic representations that form the alloy. The descriptor can be applied not only to crystalline systems but also to molecular system. We adopted 15 atomic representations: (1) atomic number, (2) atomic mass,(3) period and (4) group in the periodic table, (5) firstionization energy, (6) second ionization energy, (7) Pauling electronegativity, (8) Allen electronegativity, (9) van der Waals radius, (10) covalentradius, (11) atomic radius, (12) melting point, (13) boiling point, (14) density, and (15) specific heat. However, the compositional descriptor hardly distinguishes compounds which have different numbers of the atom because it is to regard the atomic representations of a compound as distributions of data. Therefore, the compositional descriptor cannot be applied in the case of having extrapolation in the number of components.

The rating matrix representation, which is a descriptor-free approach, shows a robust performance of recommendations for a wide variety of data sets in the Machine Learning community[11,12]. Seko et al. adopted the representation to build a recommender system for exploring currently unknown chemically relevant compositions[10]. In that work, a composition data set needs to be transformed into just two feature sets, which corresponds to users and items in a user-item rating matrix. Ratings of missing elements are approximately predicted based on the similarity of features given by the representation. To build a recommender system for HEA, we first define the candidate alloys as AB, where A and B correspond to elementary components of the alloys. We introduce two kinds of matrix representations for the eight alloys data sets. An alloy is decomposed into two elementary components with the following number of elements.

1. $|A| \in \{1, 2\}$ and $|B| \in \{1, 2, 3\}$. The numbers of possible components A and B are respectively 378 and 3303. The size of the rating matrix is (378×3303).

2. $|A| = 1$ and $|B| \in \{1, 2, 3, 4\}$. The numbers of possible components A and B are 27 and 20853, respectively. The size of the rating matrix is (27×20853).

Binary elemental descriptors is simply a binary digit representing the presence of chemical elements. The number of binary elemental descriptors corresponds to the number of element types included in the training data. In this work, the alloys data sets are composed of 27 kinds of elements; Thus, an alloy is described by a 27-dimensional binary vector with elements of one or zero.

III. TUNING HYPER-PARAMETER OF THE ERS

Because data sets used in this work are the output of calculation prediction methods, therefore we add some degree of uncertainty α in the mass function which models similarity evidence. In each data set, we use grid search to determine the α that best reproduced the alloy labels in the data set (achieving best cross-validation

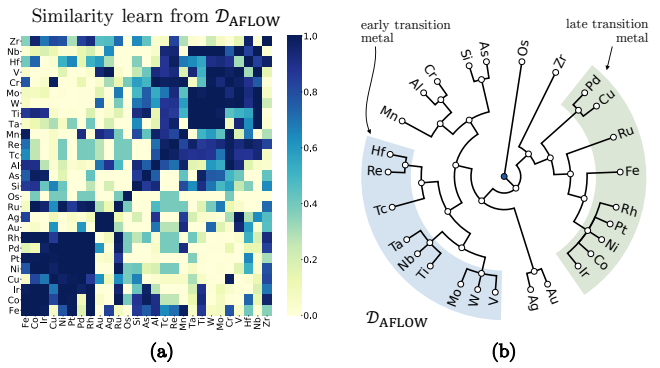

FIG. 3. (a) Heat maps for similarity matrices among 27 elements $\mathcal{E}$ obtained from$\mathcal{D}_{\mathrm{AFLOW}}$ data set. (b) Hierarchically clustered structure of all elements in $\mathcal{E}$ constructed using the similarity matrix and hierarchical agglomerative clustering. Blue and green regions indicate groups of early and late transition metals, respectively.

TABLE I. Comparison of the properties of alloys containing Zr in the two datasets $\mathcal{D}_{\mathrm{ASMI16}}$ and $\mathcal{D}_{\mathrm{CALPHAD}}$ to those predicted in $\mathcal{D}_{\mathrm{LTVC}}$ and $\mathcal{D}_{\mathrm{AFLOW}}$.

	$\mathcal{D}_{\mathrm{ASMI16}}$ 4 alloys	$\mathcal{D}_{\mathrm{CALPHAD}}$ 19 alloys
#in agreement with $\mathcal{D}_{\mathrm{AFLOW}}$	4	10
#disagreement with $\mathcal{D}_{\mathrm{AFLOW}}$	0	9
#in agreement with $\mathcal{D}_{\mathrm{LTVC}}$	3	10
#disagreement with $\mathcal{D}_{\mathrm{LTVC}}$	1	9

score). Details of the cross-validation schemes are mentioned in Section V A. The search space of α is from 0.01 to 0.9 with a step of 0.01. However, the relative magnitudes of (degree of belief HEA) and (degree of belief not HEA) are almost unchanged. In summary, the absolute value of alpha has little effect on the final result of the recommender system.

IV. DIFFERENCES BETWEEN SIMILARITY MATRICES LEARNED FROM $\mathcal{D}_{\mathrm{CALPHAD}}$ AND $\mathcal{D}_{\mathrm{AFLOW}}$

There are some notable differences between these results obtained from experiments with $\mathcal{D}_{\mathrm{CALPHAD}}$ and $\mathcal{D}_{\mathrm{AFLOW}}$. The similarity matrix learned from $\mathcal{D}_{\mathrm{AFLOW}}$ shows that Au and Ag are very similar (Figure 3 b). Furthermore, both are similar to V, Mn, and Al but not to other late transition metals (Figure 3 a). Mn is also similar to Tc, Re, and Cr but not to the other early transition metals. However, Tc and Re are somewhat similar to the other early transition metals. Furthermore, Zr is somewhat similar to the late transition metals, but different from the early transition metals. Clearly, these results are different from that obtained from $\mathcal{D}_{\mathrm{CALPHAD}}$ owing to the difference between the predicted label (HEA or $\neg HEA$) for the Zr-containing alloys recommended based on CALPHAD and AFLOW calculations, as listed in Table I. Al, Si, and As are all similar to each other and to Fe and Co (Figure 3 a). However, Al is similar to V, Cr, and Mn but not to Ti, whereas Si and As are very similar to Ti but not to V or Cr.

V. EVALUATION OF HEA-RECOMMENDATION CAPABILITY BY CROSS-VALIDATION

A. Experimental settings

Because the $\mathcal{D}_{\mathrm{ASMI16}}$ data set only contains binary alloys, we can learn a similarity matrix between the elements from a training set sampled from $\mathcal{D}_{\mathrm{ASMI16}}$. By applying the proposed process for recommending substituted alloys, we can rank all the possible binary alloys other than those in the training set. A total of 351 hypothetical binary alloys showing equivalent components can be generated from the 27 elements in $\mathcal{E}$, 45 of which are contained in $\mathcal{D}_{\mathrm{ASMI16}}$. Because no information is available for the other 306 alloys, they are ranked by the constructed model. We apply 9-fold cross-validation to $\mathcal{D}_{\mathrm{ASMI16}}$. A total of 40 out of the 45 alloys in $\mathcal{D}_{\mathrm{ASMI16}}$ are used as the training set, and the remaining 5 alloys are used as the test set to evaluate the HEA recall rate. The model learned from the 40 alloys in the training set is then used to rank the other 311 alloys, including the 5 in the test set. This cross-validation is repeated 100 times to more reliably evaluate the HEA-recommendation performance.

Because the $\mathcal{D}_{\mathrm{CALPHAD}}$ data set only contains ternary alloys, we can learn a similarity matrix between the elements or binary combinations thereof from a training set sampled from $\mathcal{D}_{\mathrm{CALPHAD}}$. We can build a model to rank all the possible ternary alloys other than those in the training set. There are 2,925 hypothetical ternary alloys showing equivalent components that can be generated from the 27 elements in $\mathcal{E}$, 243 of which are contained in $\mathcal{D}_{\mathrm{CALPHAD}}$. Because no information is available for the other 2,682 alloys, they are ranked by the constructed model. We apply 9-fold cross-validation to $\mathcal{D}_{\mathrm{CALPHAD}}$ and use 216 of the 243 alloys in $\mathcal{D}_{\mathrm{CALPHAD}}$ as the training set. The remaining 27 alloys in $\mathcal{D}_{\mathrm{CALPHAD}}$ are used as the test set to evaluate the HEA recall rate. The model learned from the 216 alloys in the training set is used to rank the other 2,709 alloys, including the 27 in the test set. This cross-validation is also repeated 100 times to more reliably evaluate the HEA-recommendation performance.

In contrast, the $\mathcal{D}_{\mathrm{ASMI16}}$, $\mathcal{D}_{\mathrm{CALPHAD}}$, $\mathcal{D}_{\mathrm{AFLOW}}$, and $\mathcal{D}_{\mathrm{LTVC}}$ data sets contain both binary and ternary alloys. Owing to the information obtained from both types of alloys, we can learn a similarity matrix between the various elements, elements and binary combinations thereof, and binary element combinations obtained from the training set sampled from $\mathcal{D}_{\mathrm{AFLOW}}$ and $\mathcal{D}_{\mathrm{LTVC}}$. We can build a

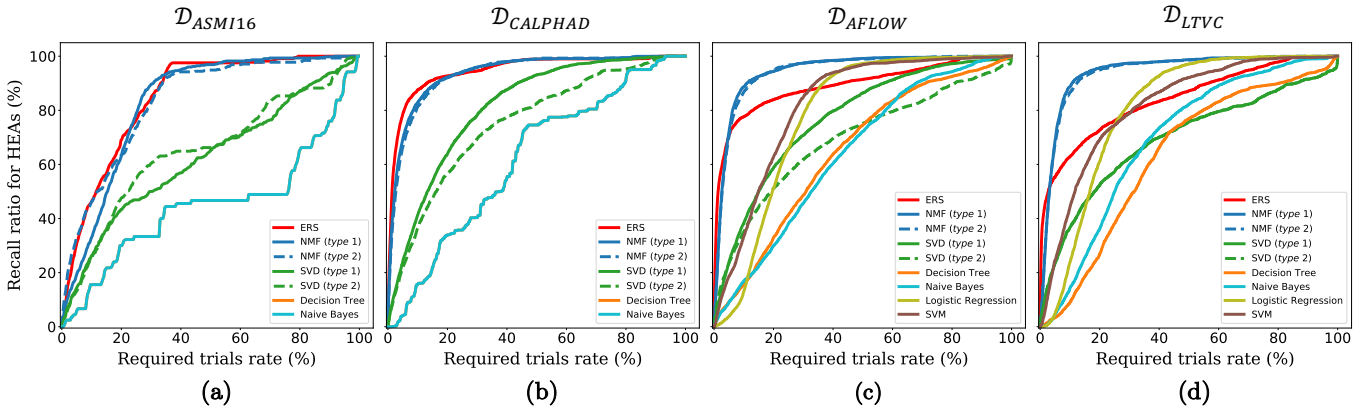

FIG. 4. Dependence of HEA recall ratio in the test sets on the number of trial required using k-fold cross-validation.

model to rank all the possible candidates for binary and ternary alloys other than those in the training set. There are 3,276 hypothetical binary and ternary alloys showing equivalent components that can be generated from the 27 elements in $\mathcal{E}$, 558 of which are contained in $\mathcal{D}_{\mathrm{AFLOW}}$. Because no information is available for the other 2,718 alloys, they are ranked by the constructed model. We apply 9-fold cross-validation to $\mathcal{D}_{\mathrm{AFLOW}}$ and use 496 of the 558 alloys in $\mathcal{D}_{\mathrm{AFLOW}}$ as the training set. The remaining 62 alloys in $\mathcal{D}_{\mathrm{AFLOW}}$ are used as the test set to evaluate the HEA recall rate. The model learned from the 496 alloys in the training set is used to rank the other 2,780 alloys including the 62 in the test set. The same evaluation method is applied to $\mathcal{D}_{\mathrm{AFLOW}}$.

A similar experiment is conducted with the $\mathcal{D}_{\mathrm{LTVC}}$ data set to evaluate the HEA-recommendation performance of the proposed ERS. Note that although the $\mathcal{D}_{\mathrm{LTVC}}$ data set contains the same alloys as the $\mathcal{D}_{\mathrm{AFLOW}}$ one, the target properties of the alloys are dissimilar because the values are estimated using different computation methods[6,7].

It should be noted that owing to the computational cost, these experiments do not use the selected alloys (i.e., those in the test set) to improve the accuracy of the HEA recommendation model for the next trial. A recommendation model based on the results of previous trials may more accurately recommend HEAs.

B. Monitoring HEA recall ratios in test set

In the experiment with $\mathcal{D}_{\mathrm{ASMI16}}$, the result shows that the ERS can significantly reduce the number of trials required to recall all the HEAs in the test set compared to the competitor systems (Figure 4 a). The proposed ERS requires less than 12, 25, and 80% of all the possible trials to recall one-half, three-quarters, and all the HEAs in the test set, respectively (Table II). In the $\mathcal{D}_{\mathrm{CALPHAD}}$ experiment, the ERS requires less than 2 and 5% of all the possible trials to recall one-half and three-quarters of the HEAs in the test set, respectively, which are the fewest trials required among all the recommender systems (Figure 4 b and Table II). Interestingly, in the $\mathcal{D}_{\mathrm{ASMI16}}$ and $\mathcal{D}_{\mathrm{CALPHAD}}$ experiments, the supervised-method-based recommender systems either approximately randomly selected possible HEAs (Naïve Bayes and decision tree) or could not rank any (logistic regression and SVM) at all because these data sets contain only positively labeled HEAs.

The result in $\mathcal{D}_{\mathrm{AFLOW}}$ experiment demonstrates that the ERS also outperforms the competitor systems in recalling one-half of the HEAs in the test set. However, the ERS cannot reliably recall the one-quarter of the HEAs remaining in the test set because not enough evidence is available in the training data to make inferences about the remaining HEAs (Figure 4 c and Table II). The $\mathcal{D}_{\mathrm{LTVC}}$ and $\mathcal{D}_{\mathrm{AFLOW}}$ experimental results are identical(Figure 4 d). Although the ERS performs better than the other recommendation systems in recovering one-half of the test HEAs in the $\mathcal{D}_{\mathrm{LTVC}}$ data set (requiring only less than 3% of the number of possible trials), it cannot reliably recover the remaining one-quarter of the test HEAs owing to the lack of evidence in the training data (Table II).

VI. EVALUATION OF HEA-RECOMMENDATION CAPABILITY BY EXTRAPOLATION

A. Experimental settings

Because $\mathcal{D}_{\mathrm{AFLOW}}$ contains both binary and ternary alloys, we can learn the similarities between the various elements and binary combinations thereof. Consequently, we can apply the ERS to $\mathcal{D}_{\mathrm{AFLOW}}$ to rank the 17,550 quaternary alloys comprising the 27 elements contained in $\mathcal{E}$. Additionally, $\mathcal{D}_{\mathrm{AFLOW}}$ and $\mathcal{D}_{\mathrm{AFLOW}}^{\mathrm{quaternary}}$ are both used to build a recommender system that ranks all the possible candidates (i.e., 80,730 alloys) for synthesizing quinary HEAs. The 754 quaternary HEAs in $\mathcal{D}_{\mathrm{AFLOW}}^{\mathrm{quaternary}}$

TABLE II. Ratio of number of trials (out of total number of possible trials) required to recall 50, 75, and 100% of HEAs in test set.

Data set	Model	Recall rates		
		Half	Three-quarters	Full
$\mathcal{D}_{\text{ASMI16}}$	ERS	**12%**	**25%**	**80%**
	NMF (type 1)	16%	25%	92%
	NMF (type 2)	13%	26%	98%
	SVD (type 1)	31%	68%	99%
	SVD (type 2)	23%	64%	99%
	Decision Tree	77%	90%	99%
	Naïve Bayes	77%	90%	99%
	Logistic Regression	-	-	-
	SVM	-	-	-
$\mathcal{D}_{\text{CALPHAD}}$	ERS	**2%**	**5%**	92%
	NMF (type 1)	3%	7%	**89%**
	NMF (type 2)	3%	8%	93%
	SVD (type 1)	14%	28%	94%
	SVD (type 2)	17	37%	93%
	Decision Tree	39%	52%	94%
	Naïve Bayes	39%	52%	94%
	Logistic Regression	-	-	-
	SVM	-	-	-
$\mathcal{D}_{\text{AFLOW}}$	ERS	**2%**	8%	97%
	NMF (type 1)	3%	**6%**	96%
	NMF (type 2)	3%	6%	**85%**
	SVD (type 1)	16%	35%	99%
	SVD (type 2)	20%	50%	99%
	Decision Tree	31%	51%	99%
	Naïve Bayes	33%	53%	99%
	Logistic Regression	20%	29%	93%
	SVM	15%	26%	99%
$\mathcal{D}_{\text{LTVC}}$	ERS	**3%**	23%	97 %
	NMF (type 1)	4%	**6%**	96%
	NMF (type 2)	4%	7%	**86%**
	SVD (type 1)	19%	49%	99%
	SVD (type 2)	19%	49%	99%
	Decision Tree	32%	48%	99%
	Naïve Bayes	26%	42%	99%
	Logistic Regression	17%	26%	89%
	SVM	12%	26%	99%

TABLE III. Ratio of number of trials (out of total number of possible trials) required to recall 50, 75, and 100% of HEAs in test set by extrapolating HEA-recommendation capability.

Data set	Model	Recall rates		
		Half	Three-quarters	Full
$\mathcal{D}_{\text{AFLOW}}^{\text{quaternary}}$	ERS	**5%**	**19%**	**99%**
	NMF (type 1)	10%	24%	99%
	NMF (type 2)	50%	67%	99%
	SVD (type 1)	13%	32%	99%
	SVD (type 2)	53%	67%	99%
$\mathcal{D}_{\text{AFLOW}}^{\text{quinary}}$	ERS	**0.4%**	**1%**	**3%**
	NMF (type 1)	10%	56%	98%
	NMF (type 2)	9%	14%	47%
	SVD (type 1)	15%	27%	99%
	SVD (type 2)	8%	57%	99%
$\mathcal{D}_{\text{LTVC}}^{\text{quaternary}}$	ERS	**13%**	**32%**	**99%**
	NMF (type 1)	14%	41%	99%
	NMF (type 2)	50%	71%	99%
	SVD (type 1)	15%	39%	99%
	SVD (type 2)	53%	71%	99%
$\mathcal{D}_{\text{LTVC}}^{\text{quinary}}$	ERS	**0.07%**	**0.2%**	**2%**
	NMF (type 1)	11%	16%	47%
	NMF (type 2)	10%	53%	93%
	SVD (type 1)	15%	27%	99%
	SVD (type 2)	7%	54%	93%

TABLE IV. List of 63 quaternary HEAs in $\mathcal{D}_{\text{LTVC}}^{\text{quaternary}}$ that no evidence about their properties is found.

FeAuRePd	AuNiPdOs	NiRePtOs	RhRePtOs	RePtOsAg
FeNiRePd	AuRhRePd	NiPdRuOs	RhPdOsAg	PdRuOsAg
FeMoOsAg	AuRhPdOs	NiPdCuOs	CoRePdRu	PdCuOsCr
FeRhPdOs	AuRePdRu	NiPdOsCr	CoRePdCu	ReCuPtOs
FeRePdRu	AuRePdCu	NiPdOsAg	CoRePdOs	RhRePdAg
FeRePdCu	AuRePdOs	MoRhPdOs	CoRePdAg	NiRePdAg
FeRePdOs	AuRePdAg	MoRePdOs	CoReRuPt	AuNiReAg
FeReRuAg	NiMoPdOs	MoRePtOs	CoRePtOs	ReRuPtOs
FeReOsAg	NiRhRePd	MoReOsAg	CoPdRuOs	RhRePdOs
FePdRuOs	NiRhPdOs	MoPdRuOs	CoRuPtOs	NiRePdOs
FePdCuOs	NiCoRePd	MoRuPtOs	RePdRuOs	FeCuOsAg
FePdOsCr	NiRePdRu	RhCoPdOs	RePdPtOs	
FeRuOsAg	NiRePdCu	RhRePdCu	RePdOsAg	

and 129 quinary HEAs in $\mathcal{D}_{\text{AFLOW}}^{\text{quinary}}$ are used to monitor the HEA recall rate for recommending quaternary and quinary HEAs, respectively. Moreover, similar experiments are conducted on the $\mathcal{D}_{\text{LTVC}}$, $\mathcal{D}_{\text{LTVC}}^{\text{quaternary}}$, and $\mathcal{D}_{\text{LTVC}}^{\text{quinary}}$ data sets to evaluate the HEA-recommendation performance of the ERS.

B. Monitoring HEA recall ratios in test set

In the $\mathcal{D}_{\text{AFLOW}}^{\text{quaternary}}$ experiment, the ERS performs significantly better than the NMF-based recommender system, requiring less than 5 and 19% of the total number of possible HEA candidates to recall 50 and 75% of the HEAs in the test set, respectively (Table III). In the $\mathcal{D}_{\text{LTVC}}^{\text{quaternary}}$ experiment, the ERS and competitor matrix-based system developed using the first type of matrix representation require 13 and 32% and 14 and 41% of the total number of possible HEA candidates to recall 50 and 75% of the HEAs in the test set, respectively (Table III). Further investigation indicates that the ERS hardly recommends any quaternary alloys in $\mathcal{D}_{\text{LTVC}}^{\text{quaternary}}$ because these alloys cannot be generated by substituting elements in any of the ternary alloys in $\mathcal{D}_{\text{LTVC}}$ (Table IV). Therefore, the properties of these alloys cannot be inferred from the ev-

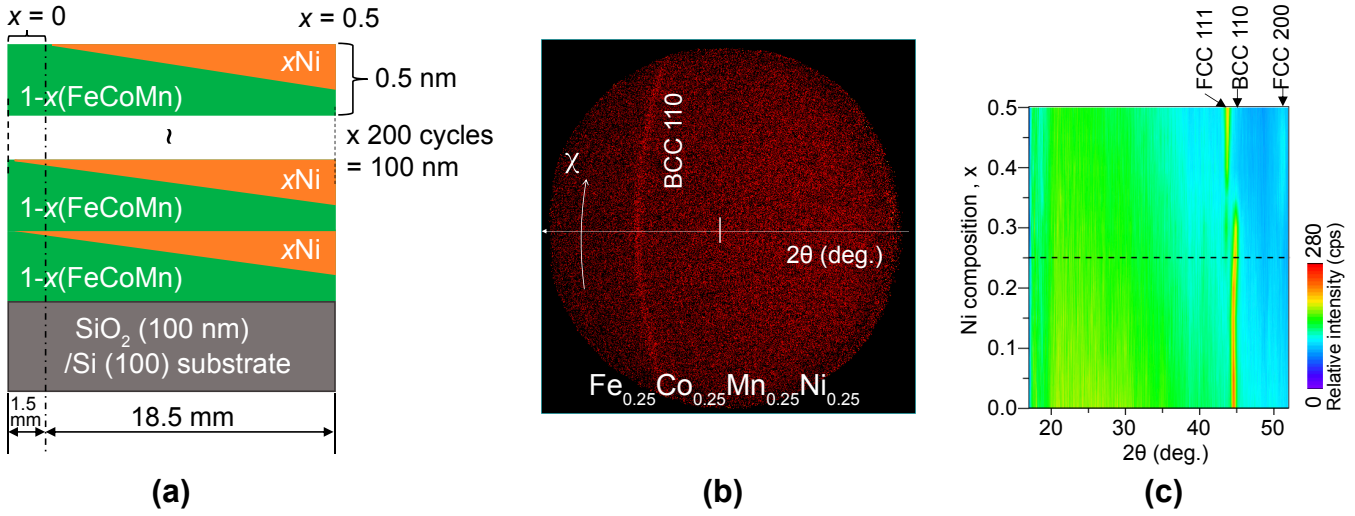

FIG. 5. (a) Schematic illustration of sample. (b) 2D-XRD image of $Fe_{0.25}Co_{0.25}Mn_{0.25}Ni_{0.25}$ film. (c) Heart mapping chat of $\omega - 2\theta$ scan converted from 2D-XRD images against Ni composition in composition spread 1-x(FeCoMn)-xNi film.

idence collected from $\mathcal{D}_{\mathrm{LTVC}}$. As a result, the rankings obtained for these alloys are significantly low; therefore, the HEA recall rate is even lower than those obtained for randomly recommended HEAs. The results obtained for $\mathcal{D}^{\mathrm{quinary}}_{\mathrm{LTVC}}$ and $\mathcal{D}^{\mathrm{quinary}}_{\mathrm{AFLOW}}$ both show that the ERS drastically outperforms the capability of the competitor systems for recommending quinary HEAs. To recall 50, 75, and 100% of the HEAs from these data sets, 10–100 times fewer trials are required using the ERS than are required using the matrix-based recommender systems (Table III).

VII. SYNTHESIS OF RECOMMENDED NOVEL FEMNCO-BASED HIGH ENTROPY ALLOYS

A. Introduction

As a case study, we fabricated a high entropy alloy film of $Fe_{0.25}Co_{0.25}Mn_{0.25}Ni_{0.25}$. Fe-Co based soft magnetic materials are widely used as inductors, transformers, and electrical machines in bulk form, and currently, the next generation high power devices require those soft magnetic applications in film form to improve abilities of high-frequency and high temperature operations[14]. For these requirements, Fe-Co based high entropy alloys are expected to achieve them.

B. Experimental section

A 100 nm thick-thermal oxidized SiO_2/Si (100) substrate was used. After the organic solvent and deionized water cleaning, the substrate was loaded in a combinatorial multi target RF-sputtering system (COMET inc., CMS-6400). To identify the stable crystal structure and its composition dependence, a composition spread film was fabricated by combinatorial method[15]. For the composition spread film, we used two targets of FeCoMn (1:1:1) and Ni (3N grade). The base pressure was below 1×10^{-5} Pa, and Ar gas pressure was set as 0.3 Pa. To adjust the deposition rate as 0.23 ± 0.01 nm/s, RF-sputtering powers of FeCoMn and Ni targets were set at 100 and 120 W, respectively. To enhance the crystallinity, the sample was annealed at 400°C for 30 min under a vacuum condition below 6×10^{-3} Pa (Advanced RIKO, MILA-3000).

Figure 5(a) shows the sample structure. The composition film layer consists of three layers. One is a single FeCoMn layer with a thickness of 0.25 nm. The other layers are composition spread film formed by FeCoMn and Ni layers. The other layers are composition spread film formed by FeCoMn and Ni layers. For the composition-spread film deposition, during the FeCoMn layer deposition, a mask moved 18.5 mm at constant speed from a point 1.5 mm from the edge of the substrate to another end where the film thickness gradually changed. After that, the targets were changed to Ni. The mask moved to the opposite direction during the Ni film deposition. The total thickness of one unit of the 1-x(FeCoMn)-xNi composition spread layer/ FeCoMn stack structure is 0.5 nm. Alternating between the three deposition steps created composition-spread region with a width of 18.5 mm. The total film thickness in the composition-spread region was set to 100 nm. The composition spread was confirmed by an X-ray fluorescence spectrometer (XRF: Shimadzu, μEDX-1400) with a measuring spot diameter of 50 μm, as shown in Fig. 6.

The crystal structure was identified by X-ray diffraction (XRD). An XRD system with a 5-kW rotating anode Cu target x-ray source and a high-resolution 2D-detector (BRUKER AXS, D8 Discover Super Speed with GADDS) was used to determine the crystal structure. The 2D-detector system can detect part of the De-

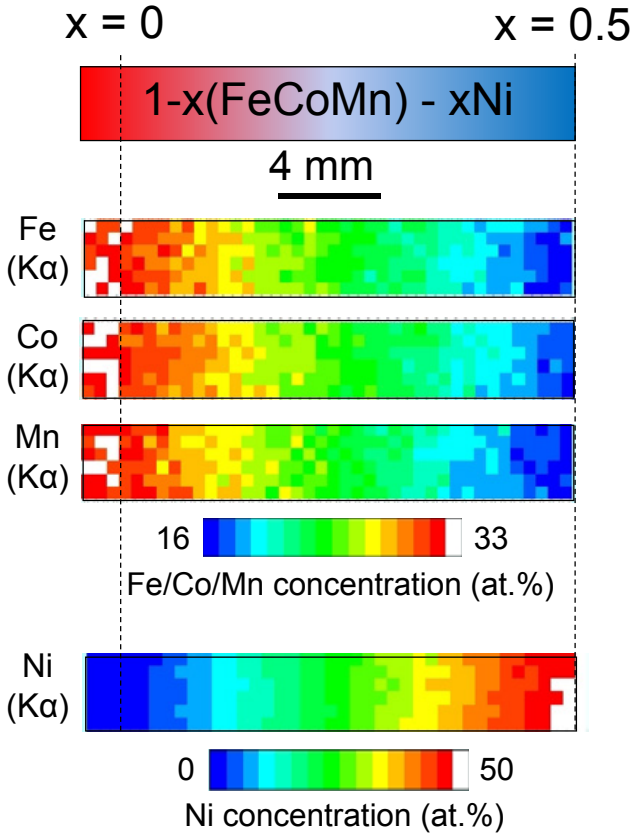

FIG. 6. Heatmapping image of Fe, Co, Mn, and Ni concentration estimated by EDX analysis. Composition was estimated from the XRF intensity of balk target materials and single-phase films of FeCoMn and Ni.

bye–Scherrer ring rapidly and two-dimensionally[16].

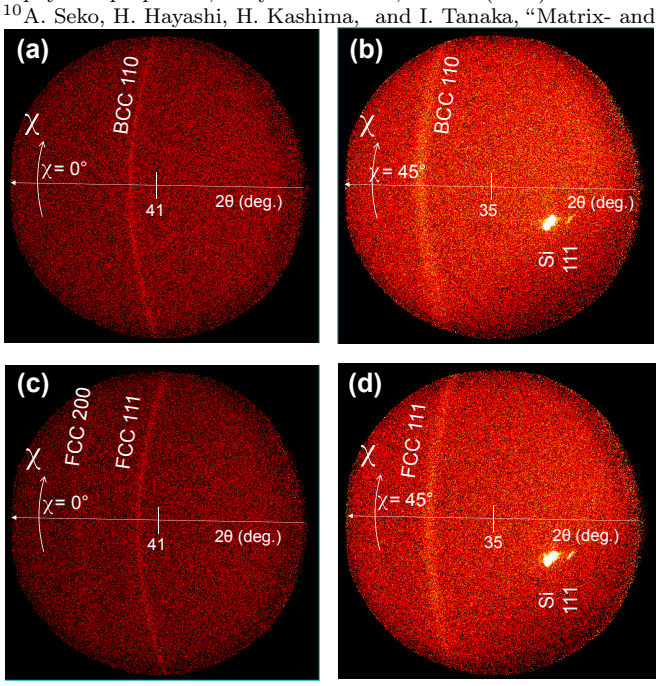

FIG. 7. 2D-XRD images at center γ angles of 0 and 45 ∘of FeCoMn-Ni films with low- (a,b) and high- (c,d) Ni concentrations. According to the powder diffraction pattern data base[13] (PDF 03-065-7519 and PDF 03-065-5131), for BCC, except for the reflection from (110), the signal intensities from other plane are not enough high to detect them in film form. So, the reflection from (110) is only detected. For FCC, in addition to the reflection from (111), the second strongest signal from (200) can barely be detected. The signals do not show no γ angle dependence, meaning the films are polycrystals in disordered crystal orientation.

[1]"Binary Alloy Phase Diagrams," in *Alloy Phase Diagrams* (ASM International, 2016) https://dl.asminternational.org/chapter-pdf/167711/a0006247.pdf.
[2]O. N. Senkov, J. D. Miller, D. B. Miracle, and C. Woodward, "Accelerated exploration of multi-principal element alloys with solid solution phases," Nature Communications **6**, 6529 (2015).
[3]D. Alman, "Searching for next single-phase high-entropy alloy compositions," Entropy **15**, 4504–4519 (2013).
[4]F. Zhang, C. Zhang, S. Chen, J. Zhu, W. Cao, and U. Kattner, "An understanding of high entropy alloys from phase diagram calculations," Calphad **45**, 1 – 10 (2014).
[5]J.-O. Andersson, T. Helander, L. Höglund, P. Shi, and B. Sundman, "Thermo-calc & dictra, computational tools for materials science," Calphad **26**, 273 – 312 (2002).
[6]C. Nyshadham, C. Oses, J. E. Hansen, I. Takeuchi, S. Curtarolo, and G. L. Hart, "A computational high-throughput search for new ternary superalloys," Acta Materialia **122**, 438 – 447 (2017).
[7]Y. Lederer, C. Toher, K. S. Vecchio, and S. Curtarolo, "The search for high entropy alloys: A high-throughput ab-initio approach," Acta Materialia **159**, 364 – 383 (2018).
[8]A. Seko, A. Togo, and I. Tanaka, "Descriptors for machine learning of materials data," in *Nanoinformatics*, edited by I. Tanaka (Springer Singapore, Singapore, 2018) pp. 3–23.
[9]A. Seko, H. Hayashi, K. Nakayama, A. Takahashi, and I. Tanaka, "Representation of compounds for machine-learning prediction of physical properties," Phys. Rev. B **95**, 144110 (2017).
[10]A. Seko, H. Hayashi, H. Kashima, and I. Tanaka, "Matrix- and tensor-based recommender systems for the discovery of currently unknown inorganic compounds," Physical Review Materials **2**, 013805 (2018).
[11]B. Sarwar, G. Karypis, J. Konstan, and J. Riedl, "Application of dimensionality reduction in recommender system - a case study," (2000).
[12]P. Symeonidis and A. Zioupos, *Matrix and Tensor Factorization Techniques for Recommender Systems*, SpringerBriefs in Computer Science (Springer, London, 2016).
[13]S. Gates-Rector and T. Blanton, "The powder diffraction file: a quality materials characterization database," Powder Diffraction **34**, 352–360 (2019).
[14]J. M. Silveyra, E. Ferrara, D. L. Huber, and T. C. Monson, "Soft magnetic materials for a sustainable and electrified world," Science **362** (2018), 10.1126/science.aao0195, https://science.sciencemag.org/content/362/6413/eaao0195.full.pdf.
[15]H. Koinuma and I. Takeuchi, "Combinatorial solid-state chemistry of inorganic materials," Nature materials **3**, 429–38 (2004).
[16]B. B. He, "Geometry and fundamentals," in *Two-dimensional X-ray Diffraction* (John Wiley & Sons, Ltd, 2018) Chap. 2, pp. 29–55, https://onlinelibrary.wiley.com/doi/pdf/10.1002/9781119356080.ch2.